Research Article

Nano Research
2022, 15(5): 4302–4309

ISSN 1998-0124 CN 11-5974/O4
https://doi.org/10.1007/s12274-022-4090-3

Anti-cancer liposomal chemophototherapy using bilayer-localized photosensitizer and cabazitaxel

Boyang Sun[1,2], Sanjana Ghosh[2], Xuedan He[2], Wei-Chiao Huang[2], Breandan Quinn[2], Meiling Tian[1], Dushyant Jahagirdar[3], Moustafa T. Mabrouk[2], Joaquin Ortega[3], Yumiao Zhang[4] (✉), Shuai Shao[1] (✉), and Jonathan F. Lovell[2] (✉)

[1] *Translational Medicine Center, The First Affiliated Hospital of Zhengzhou University, Zhengzhou 450000, China*
[2] *Department of Biomedical Engineering, University at Buffalo, State University of New York, Buffalo, NY 14260, USA*
[3] *Department of Anatomy and Cell Biology, McGill University, Montreal, Quebec H3A0C7, Canada*
[4] *School of Chemical Engineering and Technology, Tianjin University, Tianjin 300000, China*

Received: 27 July 2021 / **Revised:** 15 December 2021 / **Accepted:** 19 December 2021

ABSTRACT

Photodynamic therapy (PDT) is a non-invasive tumor ablation modality that can be enhanced in combination with concurrent chemotherapy. Previously, we demonstrated that liposomes containing a bilayer-anchored photosensitizer (porphyrin-phospholipid; PoP) can be loaded with drugs in their aqueous core to improve drug delivery and tumor ablation upon target tissue irradiation with red-light. In the present work, we demonstrate that this concept can be extended to drugs loaded within the hydrophobic bilayer of liposomes. Cabazitaxel (CTX) is a potent second generation taxane anti-cancer drug that was loaded in the bilayer of liposomes also containing 0.1 molar% PoP, generating CTX-loaded PoP liposomes (CTX-PoP-Lip). CTX-PoP-Lip showed unilamellar vesicle morphology, and exhibited integrity in storage and serum, while maintaining drug stability under laser irradiation. *In vitro* cell killing evaluation showed that red-light laser irradiation induced cytotoxicity in cells incubated with CTX-PoP-Lip, compared to control treatments. *In vivo* pharmacokinetic analysis revealed that following intravenous administration to mice, CTX and PoP exhibited somewhat altered circulation profiles, suggesting that the CTX may have exchanged with serum factors in blood. Nevertheless, when a single treatment of CTX-PoP-Lip with laser irradiation was administered to mice bearing human MIA Paca-2 tumors, tumors were effectively ablated whereas the equivalent chemotherapy and PDT monotherapies were ineffective. These results demonstrate the versatility of liposome delivery systems for achieving tumor ablation with chemophototherapy.

KEYWORDS

photodynamic therapy, cabazitaxel, liposome, chemotherapy, porphyrin-phospholipid

1 Introduction

Photodynamic therapy (PDT) is a drug-device ablation modality used for the treatment of various cancer indications [1]. The combination of PDT with chemotherapy; chemophototherapy (CPT), has been shown to lead to more effective ablation in clinical and preclinical studies [2]. Novel nanocarriers and delivery vehicles are particularly well-suited to integrate PDT photosensitizers with chemotherapeutic agents. Our lab previously has made use of liposomes incorporating small amounts of porphyrin-phospholipid (PoP) in the bilayer for CPT. The PoP photosensitizer does not exchange with serum factors and remains stably incorporated into the liposome bilayer [3]. Our prior work involved drugs loaded in the aqueous core of PoP liposomes [4–10]. However, liposomes are also able to load other cargo in the hydrophobic bilayer besides photosensitizers [11]. This is the manner that taxanes are usually formulated with liposomes and is the focus of the current study.

Taxanes are front-line chemotherapy agents for many cancer indications and have been explored preclinically as components of CPT treatments. Combination therapy has involved taxanes combined with PDT [12–16] and also photothermal therapy [17, 18]. For example, Liu and colleagues showed that by loading near infrared dyes and paclitaxel into micelles, nanoparticles (NPs) could be visualized in murine tumors with photoacoustic imaging and eradicate them with laser irradiation [19]. In another example, Zheng and co-workers demonstrated an effective PoP water/oil nanoemulsion with paclitaxel loaded in the oil core [12]. The combination CPT treatment inhibited tumor growth better than PDT or chemotherapy alone. Taking advantage of this nanoemulsions formulation, a lesser dose of paclitaxel was more efficacious.

Developed with low affinity to P-glycoprotein, cabazitaxel (CTX) is a potent second generation taxane that is active in docetaxel-resistance tumor xenografts and has been extensively explored in recent years [20]. CTX plus prednisone treatment prolonged survival of metastatic prostate cancer patients [21]. Due to its hydrophobic nature, CTX requires solubilizing excipients or drug delivery systems for administration to the blood stream. Numerous novel CTX formulations have been developed,

Address correspondence to Yumiao Zhang, ymzhang88@tju.edu.cn; Shuai Shao, sshao@zzu.edu.cn; Jonathan F. Lovell, jflovell@buffalo.edu

including serum albumin [22–26], liposomes [27–29], lipid particles [30–34], micelles [35–44], polymeric NPs [45–47], and covalent conjugates [48–52].

To date, few CTX liposome formulations have been reported, possibly owing to solubility challenges and propensity for aggregation [53]. In this study, we design a chemotherapy and phototherapy active liposome for CPT that makes use of CTX for chemotherapy and PoP for PDT. Polyethylene glycol (PEG) is included to prevent aggregation and prolong the systematic circulation [54]. The tumor inhibition effect of this CTX-PoP liposome is evaluated both *in vitro* and *in vivo*.

2 Experimental

2.1 Materials

The following lipids were obtained: Cholesterol (CordenPharma #CH-0355), 1,2-dioleoyl-sn-glycero-3-phosphocholine (DOPC, CordenPharma #LP-R4-070) and 1,2-distearoyl-phosphatidylethanolamine-methyl-polyethyleneglycol conjugate-2000 (MPEG-2000-DSPE or PEG-lipid, CordenPharma #LP-R4-039). PoP, which can be integrated into liposomes [55] was synthesized as recently reported [56]. Cabazitaxel was purchased from Carbosynth (#FC19621). Aqueous solutions were prepared using ultrapure water. Phosphate buffered saline (PBS, Dulbecco's PBS) was acquired from Gibco. Dialysis membranes were from Spectra/Por (standard RC tubing, MWCO 12–14 kD, #132700). Ethanol was from Decon (200 proof #2716)

2.2 Liposome preparation

Liposomes were composed of DOPC:CHOL:PEG:CTX:PoP at a molar ratio of 60:30:5:5:0.1. The drugs were dissolved in 1 mL ethanol at 60 °C, then the lipid solution was injected with 9 mL PBS at 60 °C. To extrude the liposomes, the lipid solution was passed 10 times through a high-pressure nitrogen extruder (Northern Lipids) with sequentially stacked 0.2, 0.1, and 0.08 μm pore size polycarbonate membranes at 60 °C. Then the solution was subjected to dialysis with phosphate buffered saline (PBS; pH 7.4) with change of buffer at least twice for 3 days. The dialyzed solution was passed through a 0.22 μm nylon filter and stored at 4 °C.

2.3 Liposome characterization

Liposome size and polydispersity index were determined with dilution in PBS by dynamic light scattering (DLS) by a NanoBrook 90 plus PALS instrument. CTX concentrations were determined by dissolving 10 μL liposomes sample in 190 μL dimethyl sulfoxide (DMSO), after sonication and vortexing, the solution was subjected to centrifugation at 5,000×*g* for 1 min and the supernatant was injected for HPLC analysis (Waters Alliance 2790 instrument). The elution gradient was from 30% to 80% acetonitrile in 0.1% trifluoroacetic acid in water at room temperature. The ultraviolet (UV) wavelength measurement of cabazitaxel was 230 nm. Fluorescence emission spectra were recorded for PoP liposomes following labeling by dissolving the liposomes in ethanol. The emission spectra were recorded with an excitation of 650 nm using a PTI fluorometer. The CTX encapsulation efficiency (EE) and loading capacity (LC) of CTX-loaded PoP liposome (CTX-PoP-Lip) were calculated as following: CTX EE% = (mass of encapsulated CTX/total mass of added CTX) × 100%; CTX LC% = (mass of encapsulated CTX/mass of NPs) × 100%.

2.4 Cryo-EM imaging

Holey carbon grids C-Flat 2/2-3Cu-T (Electron Microscopy Sciences) were washed with chloroform for 2 h before sample vitrification. Grids were treated with negative glow discharge (EMS 100 Glow Discharge System) in air at 5 mA for 15 s before the sample was applied. Sample vitrification was performed using a Vitrobot Mark IV (Thermo Fisher Scientific) which was set at 25 °C and 100% relative humidity. A sample volume of 3.6 μL was applied to the holey carbon grids and each grid was manually blotted using the Vitrobot blotting paper (standard Vitrobot Filter Paper, Ø55/20 mm, Grade 595). Then, a volume of 3.6 μL of the same sample was applied for a second time to the same holey carbon grid and the grid was blotted once in the Vitrobot for 3 s using a blot force +1, before plunging it into liquid ethane.

Data acquisition was performed using SerialEM software on the Titan Krios electron microscope at FEMR-McGill, operated at 300 kV. Images were collected with a Gatan K3 direct electron detector equipped with a Bioquantum imaging filter. Defocus ranged from −2.00 to −2.50 μm. Images were collected using a total exposure of 50 e^{-}·A^{-2} at a nominal magnification of 81,000× corresponding to a calibrated pixel size of 1.09 Å.

2.5 Reactive oxygen species (ROS) generation assay

ROS generation assay was conducted using singlet oxygen sensor green (SOSG, Thermofisher #S36002) as recently described [57]. CTX-PoP-Lip and empty PoP liposomes with 5 μg·mL^{-1} PoP concentration and PBS each containing 1 μg·mL^{-1} SOSG were irradiated with 1 mW·cm^{-2} 665 nm laser light for different time periods of 0, 0.5, 1, 3, 5, 7, or 10 min and fluorescence of SOSG was measured using a TECAN plate reader at each timepoint. The relative % ROS generation was measured by the equation: $(F_{Final} - F_{Initial})/(F_{Max} - F_{Initial}) \times 100$.

2.6 Biodistribution

Animal studies were performed in compliance with University at Buffalo IACUC protocols. Tissue biodistribution of CTX-PoP-Lip was evaluated in nude mice bearing with Mia Paca-2 tumors. Nude mice were injected 5 × 10^6 Mia Paca-2 cells on each flank to induce dual tumors. When tumor volumes reached at least ~ 100 mm^3, mice were intravenously tail injected with CTX-PoP-Lip at a dose of 10 mg·kg^{-1}. Laser irradiation was initiated 1 h post injection. Mice that received laser treatment were treated using 665 nm laser (RPMC laser, LDX-3115-665) at a laser fluence rate of 250 mW·cm^{-2} at a total fluence of 250 J·cm^{-2} while mice were anesthetized. 24 h post-administration, mice were sacrificed to collect tumors and major organs. The tissues were homogenized with 50/50 acetonitrile with water and extracted by 300 μL tert-butyl methyl ether twice. The collected tert-butyl methyl ether was dried by nitrogen, and dissolved in 150 μL 50% acetonitrile/water before LC/MS analysis.

2.7 *In vitro* drug release kinetics

The *in vitro* release of CTX from free drug solution and CTX-PoP-Lip was investigated using a dialysis membrane method. Dialysis bags (12–14 kDa MWCO) were suspended in pH 7.4 PBS containing 2% Tween 80 and maintained at 37 °C in a stirring water-bath at 100 rpm. At designated time intervals, samples of the release medium were withdrawn followed by compensation with the same volume of fresh release medium. All samples were run in triplicates. The amount of CTX released was analyzed by HPLC equipped with a C8 column.

2.8 *In vitro* cell apoptosis assay

8 × 10^4 MIA PaCa-2 tumor cells were seeded in 24-well plates overnight. The cells were treated with 5 μg·mL^{-1} CTX-PoP-Lip, empty PoP-Lip and PBS for 4 h, then irradiated with laser treatment using a 665 nm laser in a custom-built laser box at a

constant fluence rate of 10 mW·cm^{-2} at a total fluence of 10 J·cm^{-2}. Cells were incubated for 24 h and stained with Annexin V-FITC and PI (Invitrogen #V13242) according to manufacturer instruction. Flow cytometry studies were carried out using a BD LSRFortessaTM X-20 cytometer. Flowjo (version 10) software was used for data analysis.

2.9 Histology analysis

Nude mice were injected with 5 × 10^6 Mia Paca-2 cells on each flank to induce dual tumors. When the tumor volume reached 100 mm^3, mice were intravenously injected with CTX-PoP-Lip at a dose of 10 mg·kg^{-1}. Laser irradiation was initiated 1-hour post injection. Mice that received laser treatment were treated using 665 nm laser (RPMC laser, LDX-3115-665) at a laser fluence rate of 250 mW·cm^{-2} at a total fluence of 250 J·cm^{-2} while mice were anesthetized. Mice were sacrificed 72 h after the drug was injected and tumor tissue was harvested. Tumor tissue was immediately immersed in 10% formalin and was stored overnight. Tissues were then transferred to 70% ethanol and were further processed for H&E, Ki67, and TUNEL immunohistochemistry staining as recently reported [58]. Stained tumor tissue slides were imaged using Aperio Scanscope and resized using Imagescope software.

2.10 Tumor growth inhibition

Female athymic nude mice were inoculated subcutaneously with 5 × 10^6 Mia Paca-2 cells. When tumor sizes reached ~ 100 mm^3, mice were randomly grouped for treatment. The mice bearing tumors were untreated or treated by intravenous tail-vein administration of CTX-PoP-Lip with a drug dose of 10 mg·kg^{-1} CTX or empty PoP-Lip containing equivalent amounts of PoP. Laser irradiation was initiated 1-hour post injection. Mice that received laser treatment were treated using 665 nm laser (RPMC laser, LDX-3115-665) at a laser fluence rate of 250 mW·cm^{-2} at a total fluence of 250 J·cm^{-2} while mice were anesthetized. Mice were sacrificed when tumors reached 1.5 cm.

2.11 *In vitro* cell cytotoxicity and cellular uptake assay

In vitro cell assay of CTX-PoP-Lip with laser irradiation was studied with MIA PaCa-2 tumor cells. The cells were cultured and maintained at 37 °C and 5% CO_2 throughout. The media used to grow the cells included Dulbecco's modified eagle's medium supplemented with 10% fetal bovine serum and 1% Penicillin-Streptomycin. Cells were initially cultured in 25 cm^2 flasks and then seeded in a 96-well plate at a density of 1 × 10^5 cells per well and incubated for 24 h. After 24 h of incubation, the cells were washed with PBS and then treated with CTX-PoP-Lip formulation or free CTX in media at desired CTX concentrations or empty PoP-Lip in media with equivalent PoP concentrations. Then, the cells treated with laser treatment were exposed to laser using a 665 nm laser in a custom-built laser box at a constant fluence rate of 10 mW·cm^{-2} at a total fluence of 10 J·cm^{-2}. Then the cells were incubated for 24 h. To perform 2,3-bis(2-methoxy-4-nitro-5-sulfophenyl)-2H-tetrazolium-5-carboxanilide (XTT) cell viability assay, the cell culture media was removed and the cells were washed with PBS. Then, 100 µL of XTT stock solution was added to each of the 96-well plates containing cells and incubated for 2 h. The XTT stock solution was prepared by adding 100 µg·mL^{-1} of XTT and 60 µg·mL^{-1} N-methyldibenzo pyrazine methyl sulfate (PMS) in PBS. The absorbance of the plate was read at 450 nm. Cell viability was calculated as the ratio of viability of treated cells to untreated cells. All experiments were carried out in triplicate.

For the cellular uptake studies, 1 × 10^5 cells per well were cultured in 96-well plates overnight. Then the cells were washed with PBS and then treated with CTX-PoP-Lip formulation or empty PoP-Lip in media adjusted to 1 µg·mL^{-1} PoP concentration. At desired times, a 10% TX-100 surfactant solution was added to lyse the cells. The concentrations of PoP were determined fluorometrically with 420 nm excitation and 665 nm emission on a TECAN plate reader via a standard curve.

2.12 *In vivo* microdistribution of CTX-PoP-Lip

Female athymic nude mice were inoculated with 5 × 10^6 MIA PaCa-2 cells. Mice were randomly grouped and treated when the tumors grew to about 7–8 mm in diameter. Mice were intravenously injected with 10 mg·kg^{-1} CTX-PoP-Lip. A group of mice were treated with a 665 nm laser at 250 mW·cm^{-2} at total fluence of 250 J·cm^{-2} post 1 h from drug administration. All mice were sacrificed after 24 h from drug administration and tumors were harvested. The tumors were immediately flash frozen in mounting media using liquid nitrogen. The frozen tumors were then cut into thin slices of ~ 12 µm thickness using a Cryostat (H/O Bright OTF5000) machine. The imaging of PoP in tumor slices was done using a fluorescence microscope (EVOS FL Auto) with a custom filter cube having an excitation of 400 nm and an emission of 679 nm.

2.13 Pharmacokinetics

BALB/c mice were intravenously administrated liposome formulation via tail vein at 10 mg·kg^{-1} CTX concentration. The blood samples were collected from the ophthalmic vein at 0.5, 2, 4, 8, 24, and 48 h after intravenous administration. The blood samples were centrifuged at 2,000 rpm for 10 min, the serum was collected and stored at −20 °C until analysis.

To quantify CTX concentration in serum, 300 µL tert-butyl methyl ether was added to 20 µL serum, and the sample was vortexed and sonicated for 30 min until it was fully mixed. Then the sample was centrifuged at 10,000 rpm for 3 min and the tert-butyl methyl ether supernatant was collected. The extraction was repeated twice and the collected tert-butyl methyl ether was dried by nitrogen purging until dry. 150 µL 50% acetonitrile/water was added to each sample and vortexed until well-mixed. Then the sample was centrifuged at 10,000 rpm for 3 min, and the sample supernatant was transferred to HLPC vials with inserts for analysis by LC/MS.

To quantify PoP concentration, 990 µL 0.075 N HCI 90% isopropanol was mixed with 10 µL serum sample and stored at −20 °C overnight. For measurement, the samples recovered to r.t. and centrifuged at 10,000*g* for 10 min. The supernatant was collected, and the concentrations of PoP were determined fluorometrically at 665 nm via a standard curve.

2.14 LC/MS analysis of CTX

LC/MS was performed using a Sciex API 3000 triple quadrupole mass spectrometer equipped with a TurboionSpray source and a Shimadzu Prominence HPLC system. The HPLC system included 2 LC20AD pumps, an online, and a SIL-20AC autosampler. The analytical column was a Waters 2.1 ×100 mm XSelect CSH C18 column (particle size 3.5 µm). The injection volume was 10 µL, and the needle wash was 50/50 and 70/30 acetonitrile/water. The LC flow rate was 200 µL·min^{-1}. The mobile phases consisted of (A) 5/95 acetonitrile/water +0.1% formic acid, and (B) 95/5 acetonitrile/water +0.1% formic acid. The starting mobile phase was 60% B and was increased to 95% B over 5 min, it was held at 95% for 3 min before re-equilibrating for 5 min. Multiple reaction monitoring (MRM) conditions for the CTX including *m*/*z* of MRM pairs, collision energy, and orifice potential, were optimized by flow injection analysis. The MRM transitions for CTX and the deuterated internal standard (d6-cabazitaxel) were 836.7/555.5 and

842.5/561.4, respectively. The LC/MS, the dwell time of each MRM transition was 300 ms, and the pause time for scan parameter changes was 5 ms. The ion spray voltage, declustering potential, collision energy, and source temperature were 5,500 V, 22, 15, and 400 °C, respectively. The CTX quantification limit was 2.5 ng·mL^{-1}.

2.15 Data analysis

Statistical analysis was performed with GraphPad Prism 9.0. The data are presented as the means ± standard deviation (SD); the number of replicates (n) is specified in each figure. Pharmacokinetic parameters were extracted and processed with PKSolver in Excel software.

3 Results and discussion

Figure 1(a) schematically illustrates the CTX-PoP-Lip. Cholesterol and PEG-lipid were added for enhancing liposome structure stability. Hydrophobic CTX was loaded within the lipid layer via a hot ethanol injection method. The drug EE of CTX-PoP-Lip was ~ 60% and the LC of CTX was ~ 2% (Table S1 in the Electronic Supplementary Material (ESM)). Without PoP inclusion, CTX-Lip showed a similar EE and LC of ~ 58% and 2% respectively. CTX-PoP-Lip had a hydrodynamic diameter of ~ 100 nm based on DLS as shown in Fig. 1(b). Based on cryo electron microscopy imaging, CTX-PoP-Lip presented with spherical, unilamellar liposomal morphology, and consistent size with DLS measurements (Fig. 1(c)). CTX-PoP-Lip showed an optical absorption peak that was the same as PoP-Lip without CTX loading, with the characteristic PoP peak apparent at 420 nm for the PoP Soret band and 675 nm for its Q-band (Fig. 1(d)). Excited with 650 nm wavelength light, a fluorescence peak at 675 nm was observed for both CTX-PoP-Lip and PoP-Lip (Fig. 1(e)). Without PoP, CTX-Lip alone had no fluorescence character. Therefore, CTX and PoP could be loaded into well-formed liposomes that had minimal interference in physical morphology or PoP photophysical properties.

Over 3-month of storage at 4 °C, CTX-PoP-Lip remained stable with respect to nanoparticle size and maintained a low polydispersity index, demonstrating that CTX-PoP-Lip exhibited good aqueous colloidal storage stability (Figs. 2(a) and 2(b)). Given that CTX, like all taxanes, is prone to aggregation in aqueous solution, we assessed whether CTX could pass through a 0.22 μm filter. The concentration of CTX passing through to the filtrate remained stable during the 3-month storage period, providing additional evidence of CTX-PoP-Lip storage stability (Fig. 2(c)). After incubation with 50% FBS at 37 °C for 24 h, the PoP and CTX concentration showed negligible change in concentration, indicating resistance to short-term biochemical degradation in serum-like environment (Fig. 2(d)). Next, we assessed whether red light irradiation (used to excite the PoP photosensitizer) would degrade CTX, the chemotherapeutic drug component. Under the laser power of 50 mW·cm^{-2} irradiated the CTX-PoP-Lip for 2 h, the CTX did not appear to decompose under HPLC analysis, suggesting drugs are stable under laser treatment (Fig. 2(e)). The CTX release profile was assessed by dialyzing against PBS containing 1% Tween 80 at 37 °C (Fig. S1 in the ESM). CTX-PoP-Lip showed a bi-phasic release profile with faster release of 20% over the first 8 h, which might be related to CTX molecules loosely bound to the liposomes. From there, CTX exhibited a slow release over the next 48 h. Free CTX in DMSO exhibited fast release of almost 100% after 4 h, showing the permeability of the drug is not the rate determining step of the diffusion to the outer compartment in the experimental sink condition

To examine reactive oxygen species generation of CTX-PoP-Lip and empty PoP-Lip under laser irradiation, SOSG was used. SOSG is can detect and quantify production of singlet oxygen in a sample [59]. Figure S2 in the ESM illustrates the data of ROS generation. PBS with no PoP acted as a control and did not induce any fluorescence of SOSG at any time. There were minimal differences in the percent of SOSG activation by CTX-PoP-Lip and empty PoP-Lip under irradiation. The similar amount of SOSG generated by two types of liposomes under irradiation indicates that CTX did not interfere with the production of singlet oxygen generated under laser irradiation.

In vitro cellular uptake kinetics of CTX-PoP-Lip was studied in MIA Paca-2 human pancreatic cancer cells (Fig. S3 in the ESM). The PoP signal intensity indicated that CTX-PoP-Lip was untaken into cells to reach a maximum of around 5 h, a time from which ~ 0.6% uptake occurred. The *in vitro* cytotoxicity of CTX-PoP-Lip was evaluated by studying MIA Paca-2 human pancreatic cancer cells (Fig. 3). MIA Paca-2 cells were incubated with free CTX (dissolved in DMSO), CTX-PoP-Lip, or empty PoP-Lip with equivalent PoP concentrations followed by laser irradiation with 665 nm laser at a fluence rate of 10 mW·cm^{-2} at a total laser

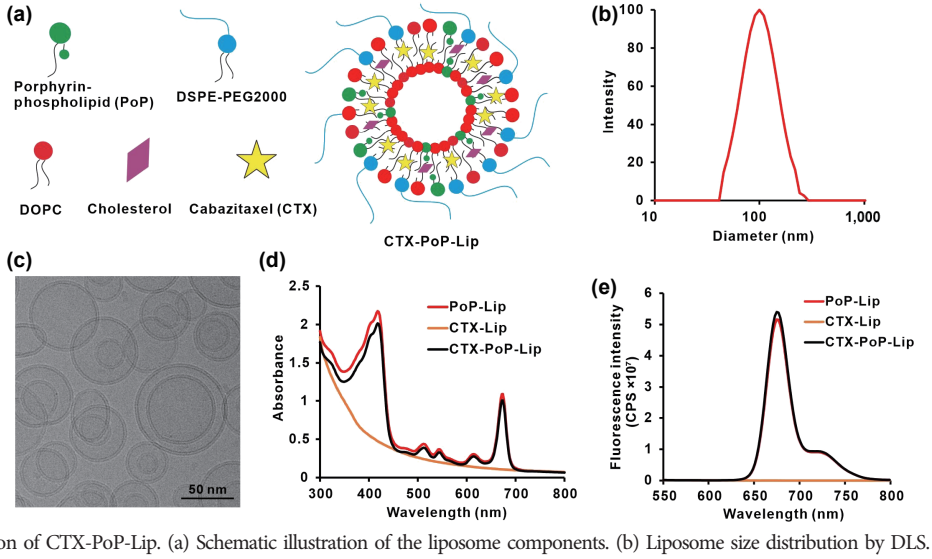

Figure 1 Characterization of CTX-PoP-Lip. (a) Schematic illustration of the liposome components. (b) Liposome size distribution by DLS. (c) Cryo-EM image of CTX-PoP-Lip. (d) Ultraviolet–visible (UV–vis) absorption spectra of indicated liposomes. (e) Fluorescence emission spectra of indicated liposomes with 650 nm excitation.

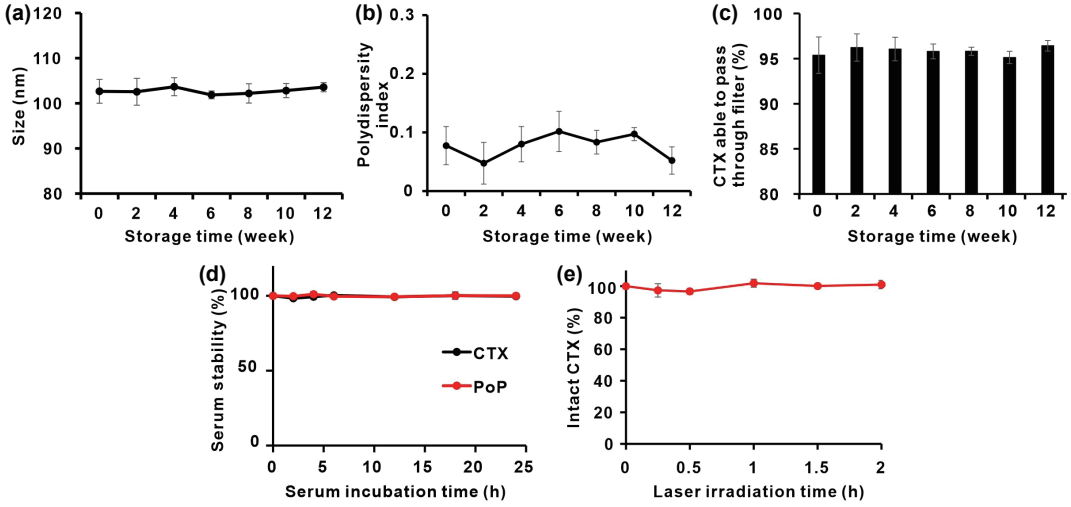

Figure 2 Stability of CTX-PoP-Lip. Storage stability of CTX-PoP-LIP stored at 4 °C. (a) Liposome size. (b) Polydispersity (PDI). (c) Amount of CTX in the CTX-PoP-Lip formulation passing through a 0.2 μm filter (d) Biochemical stability of CTX and PoP by incubating CTX-PoP-Lip in 50% FBS/PBS at 37 °C. (e) Drug stability under red laser irradiation. CTX-PoP-Lip was irradiated for 2 h under a 665 nm laser at a 50 mW·cm^{-2} fluence rate. Data show mean ± SD for n = 3 separately prepared liposome batches.

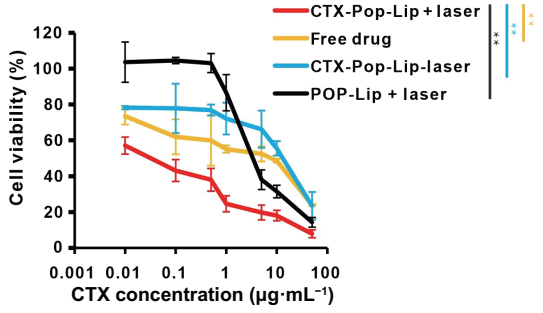

Figure 3 *In vitro* cytotoxicity of CTX-PoP-Lip. MIA PaCa-2 cells were treated with free CTX or CTX-PoP-Lip or empty Pop-Lip containing equivalent PoP concentrations. Cells that received laser treatment were irradiated using a 665 nm laser at fluence rate of 10 mW·cm^{-2} with a total fluence of 10 J·cm^{-2}. Cells were incubated for 24 h post treatment. After 24 h incubation, cell viability assay was conducted using XTT assay. At a CTX concentration at 1 μg·mL^{-1}, CTX-PoP-Lip plus laser irradiation group had a significant statistical analysis (** p < 0.05 ANOVA with Tukey's multiple comparison post-test). Data show mean ± SD for n = 5 separately prepared wells.

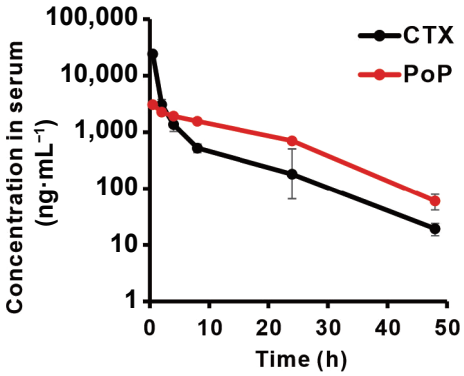

Figure 4 Pharmacokinetic behavior of CTX-PoP-Lip. Serum concentration of CTX and PoP profiles after i.v. injection of 10 mg·kg^{-1} dose of CTX-PoP-Lip in BALB/c mice. Data show mean ± SD for n = 5 separately mice.

fluence of 10 J·cm^{-2}. 24 h later, cell viability was assessed via XTT assay. CTX-PoP-Lip with laser irradiation induced strongest cytotoxicity compared to all the other groups, with a half-inhibitory concentration (IC50) value of ~ 0.05 μg·mL^{-1} CTX. However, for the other groups, the IC50 value was > 1 μg·mL^{-1}. Without laser treatment, the cytotoxicity trend of CTX-PoP-Lip was similar to free CTX. On the other hand, empty PoP-Lip with laser treatment showed a safe profile below 0.5 μg·mL^{-1} (based on the equivalent PoP concentration), but higher cytotoxicity with increasing concentration.

The mechanism of MIA PaCa-2 tumor cells killing induced by CTX-PoP-Lip CPT was evaluated by flow cytometry using an Annexin V and propidium iodide (PI) apoptosis detection kit. As showninFig. S4intheESM,CTX-PoP-Lippluslaserirradiationinduced ~ 7% necrosis while empty PoP-Lip plus laser induced ~ 2.5% and PBS had ~ 1.2% necrotic cells. For late apoptotic cells, CTX-PoP-Lip plus laser irradiation induced a similar profile as empty PoP-Lip plus laser with ~ 5.6% and 5.7% respectively, which was increased from the PBS control group of ~ 1%. The percentages of apoptotic and necrotic cells in CTX-PoP-Lip plus laser irradiation, empty PoP-Lip plus laser, and PBS group were ~ 22%, 23.1%, and 3.2%, respectively.

The pharmacokinetic behavior of CTX-PoP-Lip was studied by intravenous administration of CTX-PoP-Lip via tail vein at 10 mg·kg^{-1} CTX concentration (Fig. 4). The CTX in serum exhibited a two-phase exponential decay with a half-life of 8.3 h and AUC of 54,878 ng·mL^{-1}·h^{-1}. However, PoP exhibited a mono-exponential decay in serum and showed an 8.9 h half-life and 44, 336 ng·mL^{-1}·h^{-1} AUC. That PoP and CTX exhibited a different serum profile likely indicates that when the liposomes enter blood, the CTX at least partially exchanges with serum lipoproteins and leaves the liposome bilayer, unlike PoP, which remains stably entrapped as it is non-exchangeable. The biodistribution of the CTX in major organs was also studied in MIA PaCa-2 dual tumor-bearing nude mice (Fig. S5 in the ESM). CTX-PoP-Lip was intravenously administrated via tail vein and a single tumor received laser irradiation at 1 h. 24 h post-administration of CTX-PoP-Lip, the tumor that received laser treatment had greater CTX concentration than the one with no laser treatment.

The anti-tumor therapeutic efficacy of CTX-PoP-Lip was evaluated in mice bearing MIA-Paca-2 tumors. Female athymic nude mice were implanted with tumor cells subcutaneously and when the volume reached ~ 200 mm^3, were randomly divided into four groups. Mice were either untreated or treated with intravenous tail-vein administration of CTX-PoP-Lip at 10 mg·kg^{-1} CTX (1.45 mg·kg^{-1} PoP) or empty PoP-Lip at 1.45 mg·kg^{-1} PoP. 1 h after drug administration, a time point previously shown to be effective for CPT [60], mice that received laser treatment were treated using a 665 nm laser at a fluence rate of 250 mW·cm^{-2} at a total fluence of 250 J·cm^{-2}. Figure 5(a) shows

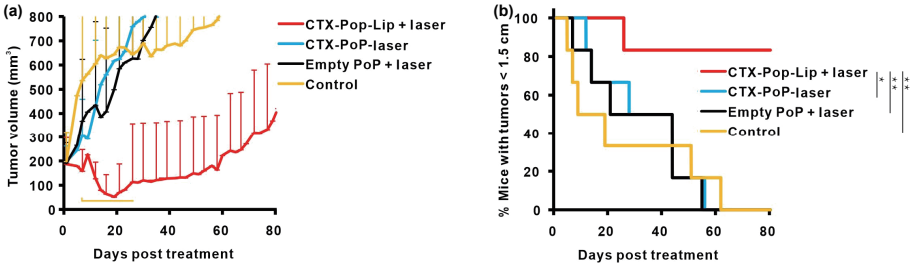

Figure 5 Tumor growth inhibition study using CTX-PoP-Lip in nude mice bearing Mia Paca-2 tumors. Mice were untreated or intravenously injected with 10 mg·kg^{-1} CTX-PoP-Lip (10 mg·kg^{-1} CTX, 1.45 mg·kg^{-1} PoP) or empty PoP-Lip (1.45 mg·kg^{-1} PoP). 1 h after drug administration, mice that received laser treatment were treated using a 665 nm laser at a laser fluence rate of 250 mW·cm^{-2} at a total fluence of 250 J·cm^{-2}. (a) Tumor volume growth curve. (b) Kaplan–Meier survival curve. Each data point show mean ± SD for n = 6 mice data obtained at each time point. Error bars show mean ± SD for n = 6 mice per group. * $p < 0.05$, ** $p < 0.01$, analyzed by log-rank test.

the anti-tumor therapeutic efficacy of CTX-PoP-Lip with laser treatment. Within 20 days of treatment, the mean tumor growth of all mice receiving CTX-PoP-Lip with laser treatment shrunk to ~ 50 mm^3 whereas mice from all other groups had a mean tumor volume ≥ 500 mm^3. This shows that mice from CTX-PoP-Lip plus laser PDT resulted in a much slower tumor growth over time compared to all other groups. The enhanced therapeutic efficacy of the combination therapy using CTX-PoP-Lip and PDT was also observed in the Kaplan-Meier Survival curve (Fig. 5(b)). On the 25th-day post treatment, 100% mice survival was observed in group that received CTX-PoP-Lip plus laser PDT, whereas ≥ 40% mice from all other groups had reached their endpoint by that time owing to much faster tumor growth and sacrifice. Except one mouse, all mice that received combination therapy of CTX-PoP-Lip plus laser PDT survived throughout 80 days of the survival study. Two mice from the CTX-PoP-Lip plus laser PDT group and one mouse from the CTX-PoP-Lip minus laser group showed no tumor recurrence. Although toxicity studies were not carried out, none of the treated mice incurred any body weight loss as shown in Fig. S6 in the ESM, suggesting that CPT using CTX-PoP-Lip is well-tolerated.

The distribution of PoP in tumors was also studied to evaluate *in vivo* anti-cancer efficacy of CTX-PoP-Lip. MIA PaCa-2 tumors were treated with 10 mg·kg^{-1} CTX-PoP-Lip mice with a 1 h laser treatment interval from drug administration. The tumors were collected 24 h after drug administration. The distribution of PoP in frozen tumor slices is shown by the green signal in the fluorescence micrographs in Fig. S7 in the ESM. Enhanced accumulation of PoP in tumors that received laser treatment was apparent compared to tumors that received no laser treatment. This supports there was better uptake of CTX-PoP-Lip in tumors that received irradiation. This further supports the mechanism for the improved tumor growth inhibition was due to enhanced delivery of CTX and PoP.

The therapeutic effects of the combination CPT treatment were probed by histological examination of tumors with hematoxylin and eosin (H&E), TUNEL, and Ki67 staining (Fig. S8 in the ESM). CPT caused cytoplasmic leakage and reduced cell density. Ki67 histology staining showed a decrease in signal, indicating a loss in viability. The increased prominence of TUNEL staining also confirmed the apoptotic effect in CPT-treated tumors.

4 Conclusions

In this work, PoP liposomes were shown to be suitable for CPT using a bilayer-loaded anti-cancer drug. The favorable liposomal storage stability, serum stability, and CTX chemical stability under laser irradiation demonstrate the potential for this approach for tumor therapy. The combination of CTX-PoP-Lip with laser treatment shows clear tumor inhibition therapeutic effects compared to equivalent PDT alone or chemotherapy alone. Unlike our prior work that involved drug release from the aqueous core of liposomes, as a hydrophobic drug, CTX is not capable of releasing easily from the bilayer. This simplifies formulation and eliminates the risk of having liposomes that have leaked their internal contents. Although tumor PK was not assessed, it is likely that vascular permeabilization induced by PDT enhanced drug delivery to tumor [61]. While many liposomal drug formulations involve active loading into the aqueous core of the liposome, this approach is relatively complex and is prone to liposome leakage. Bilayer loading is a potentially simpler liposomal formulation approach. These results demonstrate that liposomal approaches to CPT can be extended to membrane embedded photosensitizers and cytotoxic drugs with promising outcomes in a murine tumor model.

Acknowledgements

This study was supported by the National Institutes of Health (No. R01EB017270) and The National Natural Science Foundation of China (No. 82001752). The authors thank Dandan Luo for discussion and Donna M. Ruszaj for assistance with LC-MS measurements.

Conflict of interest

J. F. L. and W.-C. H. hold interest in POP Biotechnologies. Other authors declare no conflict.

Electronic Supplementary Material: Supplementary material (drug loading efficiency (Table S1), in vitro drug release (Fig. S1), ROS generation (Fig. S2), *in vitro* cellular uptake kinetics (Fig. S3), flow cytometric analysis (Fig. S4), *in vivo* biodistribution (Fig. S6), mice weight (Fig. S7), and histological study of tumor tissues (Fig. S8)) is available in the online version of this article at https://doi.org/10.1007/s12274-022-4090-3.

References

[1] Li, X. S.; Lovell, J. F.; Yoon, J.; Chen, X. Y. Clinical development and potential of photothermal and photodynamic therapies for cancer. *Nat. Rev. Clin. Oncol.* **2020**, *17*, 657–674.

[2] Luo, D. D.; Carter, K. A.; Miranda, D.; Lovell, J. F. Chemophototherapy: An emerging treatment option for solid tumors. *Adv. Sci.* **2017**, *4*, 1600106.

[3] Carter, K. A.; Luo, D. D.; Geng, J. M.; Stern, S. T.; Lovell, J. F. Blood interactions, pharmacokinetics, and depth-dependent ablation of rat mammary tumors with photoactivatable, liposomal doxorubicin. *Mol. Cancer Ther.* **2019**, *18*, 592–601.

[4] Luo, D. D.; Carter, K. A.; Razi, A.; Geng, J. M.; Shao, S.; Giraldo, D.; Sunar, U.; Ortega, J.; Lovell, J. F. Doxorubicin encapsulated in stealth liposomes conferred with light-triggered drug release. *Biomaterials* **2016**, *75*, 193–202.

[5] Luo, D. D.; Li, N.; Carter, K. A.; Lin, C. Y.; Geng, J. M.; Shao, S.;

Huang, W. C.; Qin, Y. L.; Atilla-Gokcumen, G. E.; Lovell, J. F. Rapid light-triggered drug release in liposomes containing small amounts of unsaturated and porphyrin-phospholipids. *Small* **2016**, *12*, 3039–3047.

[6] Carter, K. A.; Wang, S.; Geng, J. M.; Luo, D. D.; Shao, S.; Lovell, J. F. Metal chelation modulates phototherapeutic properties of mitoxantrone-loaded porphyrin-phospholipid liposomes. *Mol. Pharmaceutics* **2016**, *13*, 420–427.

[7] Luo, D. D.; Geng, J. M.; Li, N. S.; Carter, K. A.; Shao, S.; Atilla-Gokcumen, G. E.; Lovell, J. F. Vessel-targeted chemophototherapy with cationic porphyrin-phospholipid liposomes. *Mol. Cancer Ther.* **2017**, *16*, 2452–2461.

[8] Chitgupi, U.; Shao, S.; Carter, K. A.; Huang, W. C.; Lovell, J. F. Multicolor liposome mixtures for selective and selectable cargo release. *Nano Lett.* **2018**, *18*, 1331–1336.

[9] Miranda, D.; Carter, K.; Luo, D. D.; Shao, S.; Geng, J. M.; Li, C. N.; Chitgupi, U.; Turowski, S. G.; Li, N. S.; Atilla-Gokcumen, G. E. et al. Multifunctional liposomes for image-guided intratumoral chemo-phototherapy. *Adv. Healthc. Mater.* **2017**, *6*, 1700253.

[10] Carter, K. A.; Luo, D. D.; Razi, A.; Geng, J. M.; Shao, S.; Ortega, J.; Lovell, J. F. Sphingomyelin liposomes containing porphyrin-phospholipid for irinotecan chemophototherapy. *Theranostics* **2016**, *6*, 2329–2336.

[11] Ghosh, S.; Carter, K. A.; Lovell, J. F. Liposomal formulations of photosensitizers. *Biomaterials* **2019**, *218*, 119341.

[12] Chang, E. L.; Bu, J. C.; Ding, L. L.; Lou, J. W. H.; Valic, M. S.; Cheng, M. H. Y.; Rosilio, V.; Chen, J.; Zheng, G. Porphyrin-lipid stabilized paclitaxel nanoemulsion for combined photodynamic therapy and chemotherapy. *J. Nanobiotechnol.* **2021**, *19*, 154.

[13] Wang, X. X.; Tong, J. W.; He, Z. Y.; Yang, X. L.; Meng, F. L.; Liang, H. G.; Zhang, X. P.; Luo, L. Paclitaxel-potentiated photodynamic theranostics for synergistic tumor ablation and precise anticancer efficacy monitoring. *ACS Appl. Mater. Interfaces* **2020**, *12*, 5476–5487.

[14] Yang, X. Y.; Shi, X. Q.; Zhang, Y. N; Xu, J. K.; Ji, J. B.; Ye, L.; Yi, F.; Zhai, G. X. Photo-triggered self-destructive ROS-responsive nanoparticles of high paclitaxel/chlorin e6 co-loading capacity for synergetic chemo-photodynamic therapy. *J. Control. Release* **2020**, *323*, 333–349.

[15] Chang, J. E.; Cho, H. J.; Yi, E.; Kim, D. D.; Jheon, S. Hypocrellin B and paclitaxel-encapsulated hyaluronic acid-ceramide nanoparticles for targeted photodynamic therapy in lung cancer. *J. Photochem. Photobiol. B:Biol.* **2016**, *158*, 113–121.

[16] Gaio, E.; Conte, C.; Esposito, D.; Miotto, G.; Quaglia, F.; Moret, F.; Reddi, E. Co-delivery of docetaxel and disulfonate tetraphenyl chlorin in one nanoparticle produces strong synergism between chemo- and photodynamic therapy in drug-sensitive and -resistant cancer cells. *Mol. Pharmaceutics* **2018**, *15*, 4599–4611.

[17] Li, W. T.; Peng, J. R.; Tan, L. W.; Wu, J.; Shi, K.; Qu, Y.; Wei, X. W.; Qian, Z. Y. Mild photothermal therapy/photodynamic therapy/chemotherapy of breast cancer by Lyp-1 modified Docetaxel/IR820 Co-loaded micelles. *Biomaterials* **2016**, *106*, 119–133.

[18] Wang, D.; Zhang, S. P.; Zhang, T.; Wan, G. Y.; Chen, B. W.; Xiong, Q. Q.; Zhang, J.; Zhang, W. X.; Wang, Y. S. Pullulan-coated phospholipid and Pluronic F68 complex nanoparticles for carrying IR780 and paclitaxel to treat hepatocellular carcinoma by combining photothermal therapy/photodynamic therapy and chemotherapy. *Int. J. Nanomedicine* **2017**, *12*, 8649–8670.

[19] Zhang, Y. C.; Feng, L. Z.; Wang, J.; Tao, D. L.; Liang, C.; Cheng, L.; Hao, E. H.; Liu, Z. Surfactant-stripped micelles of near infrared dye and paclitaxel for photoacoustic imaging guided photothermal-chemotherapy. *Small* **2018**, *14*, 1802991.

[20] Vrignaud, P.; Sémiond, D.; Lejeune, P.; Bouchard, H.; Calvet, L.; Combeau, C.; Riou, J. F.; Commerçon, A.; Lavelle, F.; Bissery, M. C. Preclinical antitumor activity of cabazitaxel, a semisynthetic taxane active in taxane-resistant tumors. *Clin. Cancer Res.* **2013**, *19*, 2973–2983.

[21] De Bono, J. S.; Oudard, S.; Ozguroglu, M.; Hansen, S.; Machiels, J. P.; Kocak, I.; Gravis, G.; Bodrogi, I.; Mackenzie, M. J.; Shen, L. J. et al. Prednisone plus cabazitaxel or mitoxantrone for metastatic castration-resistant prostate cancer progressing after docetaxel treatment: A randomised open-label trial. *Lancet* **2010**, *376*, 1147–1154.

[22] Zhou, G. M.; Jin, X. Y.; Zhu, P.; Yao, J. U.; Zhang, Y. X.; Teng, L. S.; Lee, R. J.; Zhang, X. M.; Hong, W. Human serum albumin nanoparticles as a novel delivery system for cabazitaxel. *Anticancer Res.* **2016**, *36*, 1649–1656.

[23] Qu, N.; Lee, R. J.; Sun, Y. T.; Cai, G. S.; Wang, J. Y.; Wang, M. Q.; Lu, J. H.; Meng, Q. F.; Teng, L. R.; Wang, D. et al. Cabazitaxel-loaded human serum albumin nanoparticles as a therapeutic agent against prostate cancer. *Int. J. Nanomedicine* **2016**, *11*, 3451–3459.

[24] Sun, Y. T.; Zhao, Y. R.; Teng, S. S.; Hao, F.; Zhang, H.; Meng, F. C.; Zhao, X. T.; Zheng, X. L.; Bi, Y.; Yao, Y. C. Folic acid receptor-targeted human serum albumin nanoparticle formulation of cabazitaxel for tumor therapy. *Int. J. Nanomedicine* **2018**, *14*, 135–148.

[25] Qu, N.; Sun, Y. T.; Xie, J.; Teng, L. S. Preparation and evaluation of *in vitro* self-assembling HSA nanoparticles for cabazitaxel. *Anticancer Agents Med. Chem.* **2017**, *17*, 294–300.

[26] Meng, F. C.; Sun, Y. T.; Lee, R. J.; Wang, G. Y.; Zheng, X. L.; Zhang, H.; Fu, Y. G.; Yan, G. J.; Wang, Y. F.; Deng, W. Y. et al. Folate receptor-targeted albumin nanoparticles based on microfluidic technology to deliver cabazitaxel. *Cancers* **2019**, *11*, 1571.

[27] Kommineni, N.; Mahira, S.; Domb, A. J.; Khan, W. Cabazitaxel-loaded nanocarriers for cancer therapy with reduced side effects. *Pharmaceutics* **2019**, *11*, 141.

[28] Zeng, Y. Y.; Zeng, Y. J.; Zhang, N. N.; Li, C. X.; Xie, T.; Zeng, Z. W. The preparation, determination of a flexible complex liposome co-loaded with cabazitaxel and β-elemene, and animal pharmacodynamics on paclitaxel-resistant lung adenocarcinoma. *Molecules* **2019**, *24*, 1697.

[29] Mahira, S.; Kommineni, N.; Husain, G. M.; Khan, W. Cabazitaxel and silibinin co-encapsulated cationic liposomes for CD44 targeted delivery: A new insight into nanomedicine based combinational chemotherapy for prostate cancer. *Biomed. Pharmacother.* **2019**, *110*, 803–817.

[30] Ahmad, A.; Sheikh, S.; Paithankar, M.; Deshpande, G.; Lakshmaiah, K. C.; Maksud, T. M.; Khatri, A.; Manjunath, K.; Kale, P.; Patel, R. et al. Detergent and alcohol free formulation of cabazitaxel: Safety and pharmacokinetics of escalating dose of cabazitaxel lipid suspension (CLS) in patients with advanced solid maliganancies. *J. Clin. Oncol.* **2016**, *34*, e14019–e14019.

[31] Chen, W. J.; Guo, M.; Wang, S. L. Anti prostate cancer using PEGylated bombesin containing, cabazitaxel loading nano-sized drug delivery system. *Drug Dev. Ind. Pharm.* **2016**, *42*, 1968–1976.

[32] Ren, T. Y.; Wang, Q.; Xu, Y.; Cong, L.; Gou, J. X.; Tao, X. G.; Zhang, Y.; He, H. B.; Yin, T.; Zhang, H. T. et al. Enhanced oral absorption and anticancer efficacy of cabazitaxel by overcoming intestinal mucus and epithelium barriers using surface polyethylene oxide (PEO) decorated positively charged polymer-lipid hybrid nanoparticles. *J. Control. Release* **2018**, *269*, 423–438.

[33] Kommineni, N.; Saka, R.; Bulbake, U.; Khan, W. Cabazitaxel and thymoquinone co-loaded lipospheres as a synergistic combination for breast cancer. *Chem. Phys. Lipids* **2019**, *224*, 104707.

[34] Zhao, Z.; Li, Y.; Liu, H.; Jain, A.; Patel, P. V.; Cheng, K. Co-delivery of IKBKE siRNA and cabazitaxel by hybrid nanocomplex inhibits invasiveness and growth of triple-negative breast cancer. *Sci. Adv.* **2020**, *6*, eabb0616.

[35] Han, X. X.; Chen, D.; Sun, J.; Zhou, J. S.; Li, D.; Gong, F. R.; Shen, Y. L. A novel cabazitaxel-loaded polymeric micelle system with superior *in vitro* stability and long blood circulation time. *J. Biomater. Sci. Polym. Ed.* **2016**, *27*, 626–642.

[36] Zhuang, B.; Du, L.; Xu, H. X.; Xu, X. L.; Wang, C.; Fan, Y. F.; Cong, M. Y.; Yin, J. Q.; Li, H. X.; Guan, H. S. Self-assembled micelle loading cabazitaxel for therapy of lung cancer. *Int. J. Pharm.* **2016**, *499*, 146–155.

[37] Mahdaviani, P.; Bahadorikhalili, S.; Navaei-Nigjeh, M.; Vafaei, S. Y.; Esfandyari-Manesh, M.; Abdolghaffari, A. H.; Daman, Z.; Atyabi, F.; Ghahremani, M. H.; Amini, M. et al. Peptide

functionalized poly ethylene glycol-poly caprolactone nanomicelles for specific cabazitaxel delivery to metastatic breast cancer cells. *Mater. Sci. Eng. C* **2017**, *80*, 301–312.

[38] He, B.; Tan, T.; Wang, H.; Hu, H. Y.; Wang, Z. W.; Wang, J.; Li, J.; Sun, K. X.; Zhang, Z. W.; Li, Y. P. Rational design of tumor microenvironment-activated micelles for programed targeting of breast cancer metastasis. *Adv. Funct. Mater.* **2018**, *28*, 1705622.

[39] Zhong, T.; He, B.; Cao, H. Q.; Tan, T.; Hu, H. Y.; Li, Y. P.; Zhang, Z. W. Treating breast cancer metastasis with cabazitaxel-loaded polymeric micelles. *Acta Pharmacol. Sin.* **2017**, *38*, 924–930.

[40] Aydin, O.; Youssef, I.; Durmaz, Y. Y.; Tiruchinapally, G.; ElSayed, M. E. H. Formulation of acid-sensitive micelles for delivery of cabazitaxel into prostate cancer cells. *Mol. Pharmaceutics* **2016**, *13*, 1413–1429.

[41] Sun, B. Y.; Chitgupi, U.; Li, C. N.; Federizon, J.; Zhang, C. J.; Ruszaj, D. M.; Razi, A.; Ortega, J.; Neelamegham, S.; Zhang, Y. M. et al. Surfactant-stripped cabazitaxel micelles stabilized by clotrimazole or mifepristone. *Adv. Ther.* **2020**, *3*, 1900161.

[42] Sun, B. Y.; Jing, H.; Mabrouk, M. T.; Zhang, Y. M.; Jin, H. L.; Lovell, J. F. A surfactant-stripped cabazitaxel micelle formulation optimized with accelerated storage stability. *Pharm. Dev. Technol.* **2020**, *25*, 1281–1288.

[43] Zhang, Y. M.; Song, W. T.; Geng, J. M.; Chitgupi, U.; Unsal, H.; Federizon, J.; Rzayev, J.; Sukumaran, D. K.; Alexandridis, P.; Lovell, J. F. Therapeutic surfactant-stripped frozen micelles. *Nat. Commun.* **2016**, *7*, 11649.

[44] Barve, A.; Jain, A.; Liu, H.; Zhao, Z.; Cheng, K. Enzyme-responsive polymeric micelles of cabazitaxel for prostate cancer targeted therapy. *Acta Biomater.* **2020**, *113*, 501–511.

[45] Chen, Y. G.; Deng, Y. Y.; Zhu, C. Y.; Xiang, C. M. Anti prostate cancer therapy: Aptamer-functionalized, curcumin, and cabazitaxel co-delivered, tumor targeted lipid-polymer hybrid nanoparticles. *Biomed. Pharmacother.* **2020**, *127*, 110181.

[46] Fusser, M.; Øverbye, A.; Pandya, A. D.; Mørch, Ý.; Borgos, S. E.; Kildal, W.; Snipstad, S.; Sulheim, E.; Fleten, K. G.; Askautrud, H. A. Cabazitaxel-loaded Poly (2-ethylbutyl cyanoacrylate) nanoparticles improve treatment efficacy in a patient derived breast cancer xenograft. *J. Controlled Release* **2019**, *293*, 183–192.

[47] Sulheim, E.; Mørch, Y.; Snipstad, S.; Borgos, S. E.; Miletic, H.; Bjerkvig, R.; De Lange Davies, C.; Åslund, A. K. O. Therapeutic effect of cabazitaxel and blood-brain barrier opening in a patient-derived glioblastoma model. *Nanotheranostics* **2019**, *3*, 103–112.

[48] Xue, P.; Liu, D.; Wang, J.; Zhang, N.; Zhou, J. H.; Li, L.; Guo, W. L.; Sun, M. C.; Han, X. F.; Wang, Y. J. Redox-sensitive citronellol-cabazitaxel conjugate: Maintained *in vitro* cytotoxicity and self-assembled as multifunctional nanomedicine. *Bioconjugate Chem.* **2016**, *27*, 1360–1372.

[49] Bensaid, F.; Du Boullay, O. T.; Amgoune, A.; Pradel, C.; Reddy, L. H.; Didier, E.; Sablé, S.; Louit, G.; Bazile, D.; Bourissou, D. Y-shaped mPEG-PLA cabazitaxel conjugates: Well-controlled synthesis by organocatalytic approach and self-assembly into interface drug-loaded core-corona nanoparticles. *Biomacromolecules* **2013**, *14*, 1189–1198.

[50] Hoang, B.; Ernsting, M. J.; Tang, W. H. S.; Bteich, J.; Undzys, E.; Kiyota, T.; Li, S. D. Cabazitaxel-conjugated nanoparticles for docetaxel-resistant and bone metastatic prostate cancer. *Cancer Lett.* **2017**, *410*, 169–179.

[51] Xie, B. B.; Wan, J. Q.; Chen, X. N.; Han, W. D.; Wang, H. X. Preclinical evaluation of a cabazitaxel prodrug using nanoparticle delivery for the treatment of taxane-resistant malignancies. *Mol. Cancer Ther.* **2020**, *19*, 822–834.

[52] Wan, J. Q.; Qiao, Y. T.; Chen, X. N.; Wu, J. P.; Zhou, L. Q.; Zhang, J.; Fang, S. J.; Wang, H. X. Structure-guided engineering of cytotoxic cabazitaxel for an adaptive nanoparticle formulation: Enhancing the drug safety and therapeutic efficacy. *Adv. Funct. Mater.* **2018**, *28*, 1804229.

[53] Sun, B. Y.; Straubinger, R. M.; Lovell, J. F. Current taxane formulations and emerging cabazitaxel delivery systems. *Nano Res.* **2018**, *11*, 5193–5218.

[54] Suk, J. S.; Xu, Q. G.; Kim, N.; Hanes, J.; Ensign, L. M. PEGylation as a strategy for improving nanoparticle-based drug and gene delivery. *Adv. Drug Deliv. Rev.* **2016**, *99*, 28–51.

[55] Lovell, J. F.; Jin, C. S.; Huynh, E.; Jin, H. L.; Kim, C. H.; Rubinstein, J. L.; Chan, W. C. W.; Cao, W. G.; Wang, L. V.; Zheng, G. Porphysome nanovesicles generated by porphyrin bilayers for use as multimodal biophotonic contrast agents. *Nat. Mater.* **2011**, *10*, 324–332.

[56] He, X. D.; Zhou, S. Q.; Huang, W. C.; Seffouh, A.; Mabrouk, M. T.; Morgan, M. T.; Ortega, J.; Abrams, S. I.; Lovell, J. F. A potent cancer vaccine adjuvant system for particleization of short, synthetic $CD8^+$ T cell epitopes. *ACS Nano* **2021**, *15*, 4357–4371.

[57] Moukheiber, D.; Chitgupi, U.; Carter, K. A.; Luo, D. D.; Sun, B. Y.; Goel, S.; Ferreira, C. A.; Engle, J. W.; Wang, D. P.; Geng, J. M. et al. Surfactant-stripped pheophytin micelles for multimodal tumor imaging and photodynamic therapy. *ACS Appl. Bio Mater.* **2019**, *2*, 544–554.

[58] Luo, D. D.; Goel, S.; Liu, H. J.; Carter, K. A.; Jiang, D. W.; Geng, J. M.; Kutyreff, C. J.; Engle, J. W.; Huang, W. C.; Shao, S. et al. Intrabilayer ^{64}Cu labeling of photoactivatable, doxorubicin-loaded stealth liposomes. *ACS Nano* **2017**, *11*, 12482–12491.

[59] Kim, S.; Fujitsuka, M.; Majima, T. Photochemistry of singlet oxygen sensor green. *J. Phys. Chem. B* **2013**, *117*, 13985–13992.

[60] Luo, D. D.; Carter, K. A.; Geng, J. M.; He, X. D.; Lovell, J. F. Short drug-light intervals improve liposomal chemophototherapy in mice bearing MIA PaCa-2 Xenografts. *Mol. Pharmaceutics* **2018**, *15*, 3682–3689.

[61] Luo, D. D.; Carter, K. A.; Molins, E. A. G.; Straubinger, N. L.; Geng, J. M.; Shao, S.; Jusko, W. J.; Straubinger, R. M.; Lovell, J. F. Pharmacokinetics and pharmacodynamics of liposomal chemophototherapy with short drug-light intervals. *J. Control. Release* **2019**, *297*, 39–47.